



## A new trick for an old support: Stabilizing gold single atoms on LaFeO<sub>3</sub> perovskite

Chengcheng Tian<sup>b,c</sup>, Haiyan Zhang<sup>b</sup>, Xiang Zhu<sup>a,b,\*</sup>, Bo Lin<sup>b</sup>, Xiaofei Liu<sup>c</sup>, Hao Chen<sup>c</sup>, Yafen Zhang<sup>d</sup>, David R. Mullins<sup>d</sup>, Carter W. Abney<sup>d</sup>, Mohsen Shakouri<sup>g</sup>, Roman Chernikov<sup>g</sup>, Yongfeng Hu<sup>g</sup>, Felipe Polo-Garzon<sup>d</sup>, Zili Wu<sup>d</sup>, Victor Fung<sup>e</sup>, De-en Jiang<sup>e</sup>, Xiaoming Liu<sup>d</sup>, Miaofang Chi<sup>d</sup>, Jingyue Liu Jimmy<sup>f,\*\*</sup>, Sheng Dai<sup>c,d,\*\*\*</sup>

<sup>a</sup> State Key Laboratory for Oxo Synthesis and Selective Oxidation, Suzhou Research Institute of Lanzhou Institute of Chemical Physics, Chinese Academy of Sciences, Suzhou, 215123, China

<sup>b</sup> School of Resources and Environment Engineering, East China University of Science and Technology, Shanghai, 200237, China

<sup>c</sup> Department of Chemistry, University of Tennessee, Knoxville, TN 37996, United States

<sup>d</sup> Oak Ridge National Laboratory, Oak Ridge, TN 37831, United States

<sup>e</sup> Department of Chemistry, University of California, Riverside, CA 92521, United States

<sup>f</sup> Department of Physics, Arizona State University, Tempe, AZ 85287-1504, United States

<sup>g</sup> Canadian Light Source Inc., 44 Innovation Boulevard, Saskatoon, SK S7N 2V3, Canada

### ARTICLE INFO

#### Keywords:

Gold single atoms  
Perovskite  
Sintering-resistance  
Self-activating  
CO oxidation

### ABSTRACT

Single-atom catalysts (SACs) have shown great potential for achieving superior catalytic activity due to maximizing metal efficiency. The key obstacle in developing SACs lies in the availability of supports that can stabilize SACs. Here we report the first successful development of single gold (Au) atom catalysts supported on high-surface-area hierarchical perovskite oxides. The resulting Au single-atoms are extremely stable at calcination temperatures up to 700 °C in air and under reaction conditions. A high catalytic activity for CO oxidation and distinct self-activating property were also achieved. Furthermore, evidenced by theoretical calculations and experimental studies including X-ray absorption fine structures and *in situ* Fourier-transform infrared spectra, the surface Au active sites are confirmed to be predominately positively charged. This work provides a generalizable approach to fabricating highly stable Au single-atom catalysts with tunable catalytic performance, and we anticipate that this discovery will facilitate new possibilities for the development of single atom catalysts.

### 1. Introduction

Single-atom catalysts (SACs) have attracted extensive attention as a new scientific frontier, effectively bridging the fields of heterogeneous and homogeneous catalysis [1–6]. Composed of isolated metal atoms dispersed on a support, SACs display distinctly different catalytic behavior than metal nanoparticles (NPs) while simultaneously maximizing metal efficiency. As such, they offer great potential for achieving superior catalytic activity and selectivity, particularly for systems based on noble metals [7–12]. However, it has been well documented that the surface free energy of metals increases significantly with decreasing particle size, promoting aggregation or

sintering during synthetic procedures [13–15]. Therefore, while the synthesis of uniform and stable single-atom catalysts is highly desired, it nevertheless remains a grand challenge.

The most common approach to SACs preparation involves tuning conventional chemical methods to anchor single metal atoms on special sites of supports. This is generally accomplished by enhancing the metal-support interactions [8,10,11,16–20], providing effective voids [21,22] or surface vacancy defects in the supports (TiO<sub>2</sub>, CeO<sub>2</sub>) [7,19,23–25]. As these sites help to stabilize the atomically-dispersed metal atoms, the properties of the resulting SACs are highly dependent upon the selection of support. The first practically synthesized single-atom catalyst Pt/FeOx [8,16], as well as its analogues Ir/FeOx [17] and

\* Corresponding author at: State Key Laboratory for Oxo Synthesis and Selective Oxidation, Suzhou Research Institute of Lanzhou Institute of Chemical Physics, Chinese Academy of Sciences, Suzhou, 215123, China.

\*\* Corresponding author.

\*\*\* Corresponding author at: Department of Chemistry, University of Tennessee-Knoxville, TN 37996, United States.

E-mail addresses: [xiang@licp.cas.cn](mailto:xiang@licp.cas.cn) (X. Zhu), [jingyue.Liu@asu.edu](mailto:jingyue.Liu@asu.edu) (J. Liu Jimmy), [dais@ornl.gov](mailto:dais@ornl.gov) (S. Dai).

<https://doi.org/10.1016/j.apcatb.2019.118178>

Received 6 June 2019; Received in revised form 5 September 2019; Accepted 7 September 2019

Available online 09 September 2019

0926-3373/ © 2019 Elsevier B.V. All rights reserved.

Au/CeO<sub>2</sub> [18], exhibit strong covalent metal-support interactions. In this respect, due to their high thermal stability and ideal ABO<sub>3</sub>-type crystal structure, perovskite oxides have been reported to profoundly enhance the stability of precious metals [26–28] and could function as promising supports for preparing single atom catalysts. However, to the best of our knowledge there have been no reports of perovskite oxide-supported single metal atoms.

With these considerations in mind, we report the first successful fabrication of a novel class of supported Au SACs, leveraging a heterostructured perovskite to provide a unique nanoarchitecture for the immobilization of SACs. The resulting Au single-atom catalysts not only exhibit sintering-resistance at a high temperature of 700 °C but also show high catalytic activity towards CO oxidation and distinctively self-activating under reaction conditions. Evidenced by theory calculations and experimental results, the surface Au active sites are confirmed to be predominately positively charged. We anticipate that this new study could inspire the discovery of other perovskite-supported metal single atom catalysts, and thus advance their catalytic applications.

## 2. Experimental section

### 2.1. Catalyst preparation

The perovskite support (LaFeO<sub>3</sub>/MCF) was prepared by a modified Pechini-method [29,30]. Typically, La(NO<sub>3</sub>)<sub>3</sub>·6H<sub>2</sub>O (0.165 mmol) and Fe(NO<sub>3</sub>)<sub>3</sub>·9H<sub>2</sub>O (0.165 mmol) were dissolved in dilute HNO<sub>3</sub> under vigorous stirring, the pH value of the solution was kept between two and three. Then 10 mL of a water-ethanol (v/v = 1:7) solution containing citric acid (0.66 mmol) as a chelating agent for the metal ions was added to the reaction. The molar ratio of metal ions to citric acid was 1:2. As a cross-linking agent, ethylene glycol was added with a final concentration of 0.20 g mL<sup>-1</sup>. The solution was stirred for 2 h to form a sol, and then the MCF (0.2 g) was added under stirring. The suspension was further stirred for another 4 h, and then the temperature was then increased to 70 °C and placed under vacuum to completely evaporate solution. Then the dried samples were heated to 500 °C with a heating rate of 1 °C min<sup>-1</sup> and held at 500 °C for 2 h in air and was further heated to 700 °C for 2 h in air with a heating rate of 1 °C min<sup>-1</sup>.

The Au precursor was introduced onto the LaFeO<sub>3</sub>/MCF support using a DP method [31]. Typically, 0.01 g of hydrogen tetrachloroaurate (III) trihydrate (HAuCl<sub>4</sub>·3H<sub>2</sub>O) was dissolved into 4 mL deionized water. The pH value of the resulting solution was adjusted to 10 using a solution of 1.0 mol L<sup>-1</sup> NaOH under vigorous stirring at room temperature. Subsequently, the as-synthesized LaFeO<sub>3</sub>/MCF support was added and the pH value was controlled at 10 by the further addition of NaOH solution. The mixed solution was stirred for an additional 2 h in an 80 °C water bath. Finally, the precipitates were separated by centrifugation and washed several times with deionized water. The product was dried at 50 °C in vacuum overnight to obtain Au loaded LaFeO<sub>3</sub>/MCF pre-catalysts.

### 2.2. Catalyst characterization

The powder XRD data were recorded with a PANalytical Empyrean diffractometer, operated at 45 kV and 40 mA (scanning step: 0.02° per step). The diffraction patterns were recorded in the range of 10–80°. The LaFeO<sub>3</sub> nanoparticle size was estimated according to Scherrer equation:  $d = K\lambda / (\beta \cos\theta)$  ( $K = 0.9$ ,  $\lambda = 0.1540598$  nm), where  $K$  is the shape factor,  $\lambda$  is the X-ray wavelength,  $\beta$  is the line broadening at half the maximum intensity (FWHM) in radians, and  $\theta$  is the Bragg angle. The nitrogen adsorption and desorption isotherms were measured at 77 K under a Gemini 2375 surface area analyzer. Transmission electron microscope (TEM) and Z-contrast scanning transmission electron microscope (STEM) experiments were conducted on HITACH HD2000 microscopes with an accelerating voltage of 200 kV. Aberration-corrected high-angle annular dark-field scanning

transmission electron microscopy (HAADF-STEM) was conducted on a JEOL JEM-ARM 200F at an acceleration voltage of 200 kV equipped with a CEOS probe corrector (Heidelberg, Germany) to provide a guaranteed image resolution of 0.08 nm. Energy-dispersive X-ray spectroscopy (EDS) were performed on a JEOL JEM 2200FS STEM/TEM microscope at an acceleration voltage of 200 kV equipped with a CEOS probe corrector (Heidelberg, Germany) to provide nominal resolution of ~0.07 nm. A Bruker-AXS silicon drift detector (SDD) was used for all EDS elemental analysis. Elemental analysis of the samples was done by inductively coupled-plasma atomic emission spectroscopy (ICP-AES) using Optima 2100 DV spectrometer (PerkinElmer Corporation). X-ray photoelectron spectroscopy (XPS) measurements: XPS experiments were performed with a PHI 3056 spectrometer equipped with an Al anode source operated at 15 KV and an applied power of 350 W and a pass energy of 93.5 eV.

### 2.3. X-ray absorption fine structure (XAFS) studies

The XAS data was recorded at the Au L<sub>III</sub>-edge (11,919 eV) at beamline 2-2 at the Stanford Synchrotron Radiation Laboratory, SLAC National Accelerator Laboratory. Si (111) double crystal monochromator was used and detuned by 20% to reject higher harmonics. The Au XAS was measured in fluorescence mode using a 13-element, fast count rate, high resolution Ge detector (Canberra), placed perpendicular to the beam path. Ion chambers for measuring the incident beam (I<sub>0</sub>), transmission (I<sub>t</sub>) and an Au foil for energy reference (I<sub>ref</sub>) were measured simultaneously. I<sub>0</sub> was filled with N<sub>2</sub> and I<sub>t</sub> and I<sub>ref</sub> were filled with Ar. The Au absorption was measured out to  $k = 16$ .

The sample were ground to a fine powder, mixed with BN and pressed into a 13 mm diameter pellet. The absorbance of the analyte,  $\mu(x)$ , was ca. 0.01–0.02. The pellet was mounted in a Nashner-Adler reaction cell [32]. A gas flow pipe terminated near the sample's surface to allow *in situ* studies of temperature and gas-flow controlled experiments. All XAS measurements were made with the cell filled with He at 25 °C.

The programs ATHENA and ARTEMIS (available through the DEMETER software package, version 0.9.25) were used to reduce and fit the data, respectively [33]. Data reduction consisted of pre-edge subtraction, background determination, normalization and spectral averaging. The  $k^1$ -,  $k^2$ - and  $k^3$ -weighted  $X(k)$  were Fourier transformed and fit in  $R$  space. Due to the relatively poor signal to noise resulting from the low Au concentration the EXAFS was fit from  $k = 3$ –12. The  $k$ -space EXAFS spectra of Au<sub>1</sub>/LaFeO<sub>3</sub>/MCF, Au foil and Au<sub>2</sub>O<sub>3</sub>, which were collected using the BioXAS beamline. (Fig. S1).

### 2.4. Catalytic CO oxidation

Catalytic CO oxidation was carried out in a fixed-bed reactor (straight quartz tube) at atmospheric pressure. For the measurement of CO light-off curves showing CO conversion as a function of reaction temperature and the long-term *in operando* stability, a 20 mg catalyst supported by quartz wool was loaded in the reactor. The feed gas of 1% CO balanced with dry air (< 4 ppm water) passed through the catalyst bed at a flow rate of 10 mL/min corresponding to gas hourly space velocity (GHSV) of 30,000 mL (h g<sub>cat</sub>)<sup>-1</sup>. Prior to the catalytic test, each catalyst was calcined in an oven under air at 700 °C for 2 h. The concentrations of CO and CO<sub>2</sub> in the reactor effluent were analyzed by a Buck Scientific 910 gas chromatograph equipped with a dual molecular sieve/porous polymer column (Alltech CTR1) and a thermal conductivity detector.

### 2.5. In situ infrared study

The adsorption of CO followed by FTIR spectroscopy was performed using a Thermo Nicolet Nexus 670 FTIR spectrometer with an MCT detector, while the effluent stream was monitored by a Pfeiffer Vacuum

GSD 301 O<sub>2</sub> mass spectrometer. Each spectrum was recorded with 64 scans at a resolution of 4 cm<sup>-1</sup>. A ceramic cup with the catalyst sample was inserted into a diffuse reflectance infrared transform spectroscopy (DRIFTS) cell (HC-900, Pike Technologies). The samples (Au<sub>1</sub>/LaFeO<sub>3</sub>/MCF and LaFeO<sub>3</sub>/MCF) were pretreated at 340 °C under 35 mL min<sup>-1</sup> of 4% O<sub>2</sub>/He for 1 h. After pretreatment, the sample was cooled down to 6 °C under 30 mL min<sup>-1</sup> of He. A background spectrum was collected before chemisorption. 30 mL min<sup>-1</sup> of 2%CO/(Ar + He) were flowed over the catalyst for approximately 10 min, then the CO adsorbed on the surface was desorbed with a flush of 30 mL min<sup>-1</sup> of He. Spectra were collected after 3 min of desorption.

## 2.6. Theoretical calculation

Density functional theory calculations were performed using the Vienna Ab-initio Simulation Package (VASP) [34,35]. The Perdew-Burke-Ernzerhof (PBE) [36] form of the generalized-gradient approximation (GGA) was used for electron exchange and correlation energies. All calculations were performed with spin polarization. The projector-augmented wave method was used to describe the electron-core interaction [34,37], and the kinetic energy cutoff was set to be 450 eV. A 3 × 3 × 1 and 3 × 2 × 1 sampling of Brillouin zone with a Monkhorst-Pack scheme was used for LaFeO<sub>3</sub> and TiO<sub>2</sub>, respectively [38]. The top two layers of the slabs were allowed to relax in all calculations. The cluster absorption energy (E<sub>ads</sub>) was calculated with the equation E<sub>ads</sub> = E<sub>surface + Aux</sub> - (E<sub>surface</sub> + E<sub>Aux</sub>). The energies of E<sub>Aux</sub> was computed by placing the adsorbate in a cubic cell with a 15 Å wide vacuum in each direction; the gas phase Au<sub>4</sub> geometry used is the global minimum planar configuration.

Au adsorption was tested on the predicted stable (001) B termination of LaFeO<sub>3</sub>, shown in Fig. S2. Adsorption energies and Bader charges are compiled in Table S2. It was found that configurations resulting in Au–O bonding exhibited a positive Au Bader charge, whereas those with Au–Fe bonding had a negative Bader charge as a result of the electronegativity differences. Au single atoms with negative Bader charges exhibited much weaker adsorption energies than the positive counterparts. Although configuration A has the strongest CO adsorption energy, it only weakly adheres to the surface and is an unlikely candidate for the SAC species observed experimentally. Only configuration C shown has a reasonable binding energy with the surface and with CO which is observed experimentally. A strong binding of CO with Au can be explained by the Bader charge, with the positive (oxidized) Au species exhibiting good catalytic behavior similar to that of its leftward neighbors, such as Pt.

## 3. Results and discussion

### 3.1. Catalyst synthesis and characterization

The diagram shown in Fig. 1 depicts the facile synthesis of the Au SACs. The LaFeO<sub>3</sub>/MCF support was synthesized by a modified Pechini-method [29], while the Au species was subsequently introduced by a deposition-precipitation (DP) method using HAuCl<sub>4</sub> in water, affording about 0.3 wt% loading. The Au loaded LaFeO<sub>3</sub>/MCF pre-catalysts were calcined at 700 °C in air for 2 h to form the final catalyst, denoted as Au<sub>1</sub>/LaFeO<sub>3</sub>/MCF. The mesoporosity of the Au<sub>1</sub>/LaFeO<sub>3</sub>/MCF was evaluated by surface area measurements, which exhibited Type IV isotherms (Fig. S3), a BET surface area of 407 m<sup>2</sup> g<sup>-1</sup>, and a total pore volume of 1.55 cm<sup>3</sup> g<sup>-1</sup> (Table 1). As measured by inductively coupled plasma atomic emission spectroscopy (ICP-AES), the La, Fe and Au loadings in the Au<sub>1</sub>/LaFeO<sub>3</sub>/MCF are 9.5, 3.7 and 0.3 wt %, respectively, affording an atomic ratio of La to Fe of almost precisely 1: 1. X-ray diffraction (XRD) patterns of the LaFeO<sub>3</sub>/MCF and the Au<sub>1</sub>/LaFeO<sub>3</sub>/MCF reveal broad peaks corresponding to small crystallites of LaFeO<sub>3</sub>, as displayed in Fig. S4. Importantly, Au diffraction peaks were not observed for the Au<sub>1</sub>/LaFeO<sub>3</sub>/MCF, even after calcination treatments at

temperatures as high as 700 °C. The XRD studies also demonstrate the remarkable resistance to sintering displayed by the Au<sub>1</sub>/LaFeO<sub>3</sub>/MCF system. The transmission electron microscopy (TEM, Fig. S5) and the Z-contrast scanning transmission electron microscopy (STEM, Fig. 2a) images of the Au<sub>1</sub>/LaFeO<sub>3</sub>/MCF clearly reveal the morphology of the mesoporous MCF and the conforming ultrathin layer of LaFeO<sub>3</sub> coating the interior walls of the MCF (black arrows).

In an effort to characterize the dispersed state of the Au species, aberration-corrected high-angle annular dark-field STEM (HAADF-STEM) and was further employed, with a representative image and intensity profiles displayed in Figs. 2b and S6. As expected, a large number of randomly dispersed atomic Au species were observed, highlighted by the white circles. A detailed energy-dispersive X-ray spectroscopy (EDS) elemental mapping measurement (Fig. S7) of the Au<sub>1</sub>/LaFeO<sub>3</sub>/MCF shows the coexistence of Au, La, Fe and Si signals throughout the analyzed regions. The TEM and STEM results corroborate the results obtained from the XRD studies, confirming the atomic dispersion of the Au species on LaFeO<sub>3</sub>/MCF, even after a high-temperature calcination process.

To further confirm that our synthesized catalysts contained only atomically-dispersed individual Au atoms throughout the whole catalyst, we performed X-ray adsorption fine structure (XAFS) spectroscopy (Fig. S1). The X-ray absorption near edge spectra (XANES) of Au<sub>1</sub>/LaFeO<sub>3</sub>/MCF, Au-foil and Au<sub>2</sub>O<sub>3</sub> are shown in Fig. 2c. The Au<sub>1</sub>/LaFeO<sub>3</sub>/MCF shows an intense peak near 11,921 eV. The pronounced “white line” is attributable to depletion of Au *d* orbitals from their metallic *d*<sup>10</sup> configuration [39], indicating the perovskite-supported Au species possesses appreciable oxidic character resembling that of the Au<sup>3+</sup> in Au<sub>2</sub>O<sub>3</sub>. To get a better understanding of the Au coordination environment, XANES data were compared against reference spectra from Au-foil, Au-chlorides, Au-sulfides, and Au-hydroxides (Fig. S8). While all oxidized Au species display the characteristic white line, the absorption edge and spectral shape of the Au<sub>1</sub>/LaFeO<sub>3</sub>/MCF is closest to those of the Au(OH)<sub>3</sub> or Au<sub>2</sub>O<sub>3</sub> species, suggesting a local coordination environment composed of oxygen atoms [40].

Extended X-ray absorption fine structure (EXAFS) spectra were also analyzed for the Au<sub>1</sub>/LaFeO<sub>3</sub>/MCF, as shown in Fig. 2d. Qualitatively, it can be seen that for the Au<sub>1</sub>/LaFeO<sub>3</sub>/MCF system there is an intense peak below 0.2 nm, consistent with scattering along an Au–O path. As importantly, the Au foil displays a characteristic Au–Au scattering path at 0.3 nm which is absent in both Au<sub>1</sub>/LaFeO<sub>3</sub>/MCF and Au<sub>2</sub>O<sub>3</sub>. The first shell scattering of Au<sub>1</sub>/LaFeO<sub>3</sub>/MCF was fit using the ARTEMIS program [33,41] to determine the average coordination number and positions of the nearest neighbors, shown in Table S3. Au has essentially four O nearest neighbors near 0.2 nm as in Au<sub>2</sub>O<sub>3</sub>. While we can't definitively exclude the possibility of Au–Au scattering, inclusion of this scattering path in the fit did not improve the quality of the fit. Taken comprehensively all above characterizations, the oxidized Au character, spectral similarity to oxygen-surrounded Au species, and the lack of Au–Au interactions supports the predominance of atomically dispersed individual Au atoms supported on the perovskite.

### 3.2. Catalytic activity: CO oxidation

CO oxidation was employed as a probe reaction because of its fundamental importance and practical utility [42–47]. Fig. 3a presents a comparison of the light-off curves for CO oxidation by the LaFeO<sub>3</sub>/MCF support and Au<sub>1</sub>/LaFeO<sub>3</sub>/MCF after calcination at 700 °C in air. Although the pristine LaFeO<sub>3</sub>/MCF material showed no activity below 200 °C, introduction of the single Au atoms results in a significantly enhanced activity. The turnover frequency (TOF) of the 700 °C-calcined Au<sub>1</sub>/LaFeO<sub>3</sub>/MCF reaches 0.025 mol<sub>CO</sub> mol<sub>Au</sub><sup>-1</sup> s<sup>-1</sup> at 25 °C, which is more than four-times greater than the 0.006 mol<sub>CO</sub> mol<sub>Au</sub><sup>-1</sup> s<sup>-1</sup> of the 700 °C-calcined Au–TiO<sub>2</sub> catalyst standard (World Gold Council) under the same conditions. The catalytic performance is also comparable to typical reported Au SACs (Table S1). It is noteworthy that the onset of

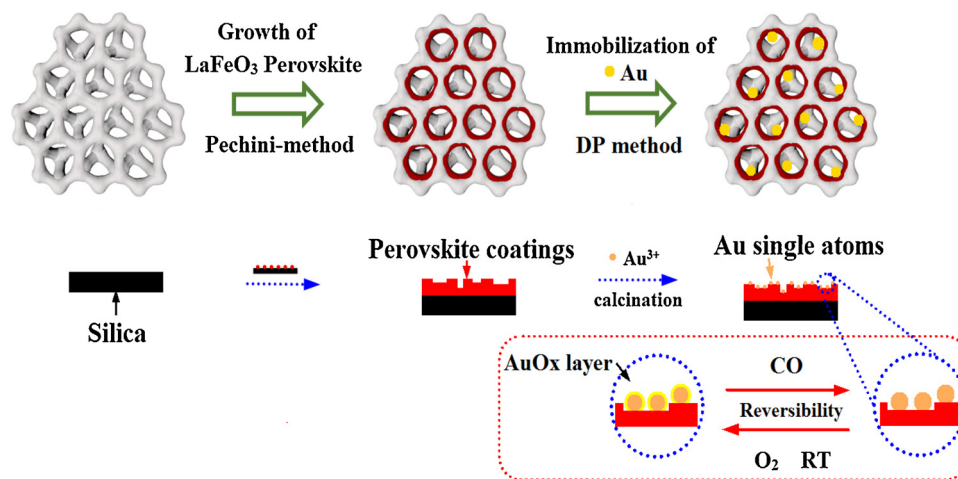


Fig. 1. Schematic illustration of the  $\text{Au}_1/\text{LaFeO}_3/\text{MCF}$  preparation process.

**Table 1**  
Textural properties and composition of the catalysts.

| Catalyst                                | $S_{\text{BET}}^{\text{a}}$ ( $\text{m}^2 \text{g}^{-1}$ ) | $V_{\text{total}}^{\text{a}}$ ( $\text{cm}^3 \text{g}^{-1}$ ) | $\text{Au}^{\text{b}}$ (wt%) |
|---|--|---|------------------------------|
| MCF                                     | 736  | 2.36  | 0                            |
| $\text{LaFeO}_3/\text{MCF}$             | 465  | 1.71  | 0                            |
| $\text{Au}_1/\text{LaFeO}_3/\text{MCF}$ | 407  | 1.55  | 0.3                          |

<sup>a</sup> Determined from nitrogen sorption recorded at 77 K.

<sup>b</sup> Determined by ICP-AES.

catalytic CO oxidation by  $\text{Au}_1/\text{LaFeO}_3/\text{MCF}$  was so abrupt, with a conversion dramatically increasing to 100% at 170 °C, whereas conversion was only slightly higher than 20% at 150 °C. The similar behavior of the  $\text{Au}_1/\text{LaFeO}_3/\text{MCF}$  catalysts as a function of calcination temperature (300 °C and 500 °C) were also observed (Fig. S9). Such a sudden change in catalytic activity usually reflects structural changes of the active sites or the activation of new catalytic centers. To conform this special behavior, this catalyst was also evaluated by performing three consecutive catalytic runs (Fig. S10). No appreciable deactivation was detected after three consecutive catalytic runs and the second and

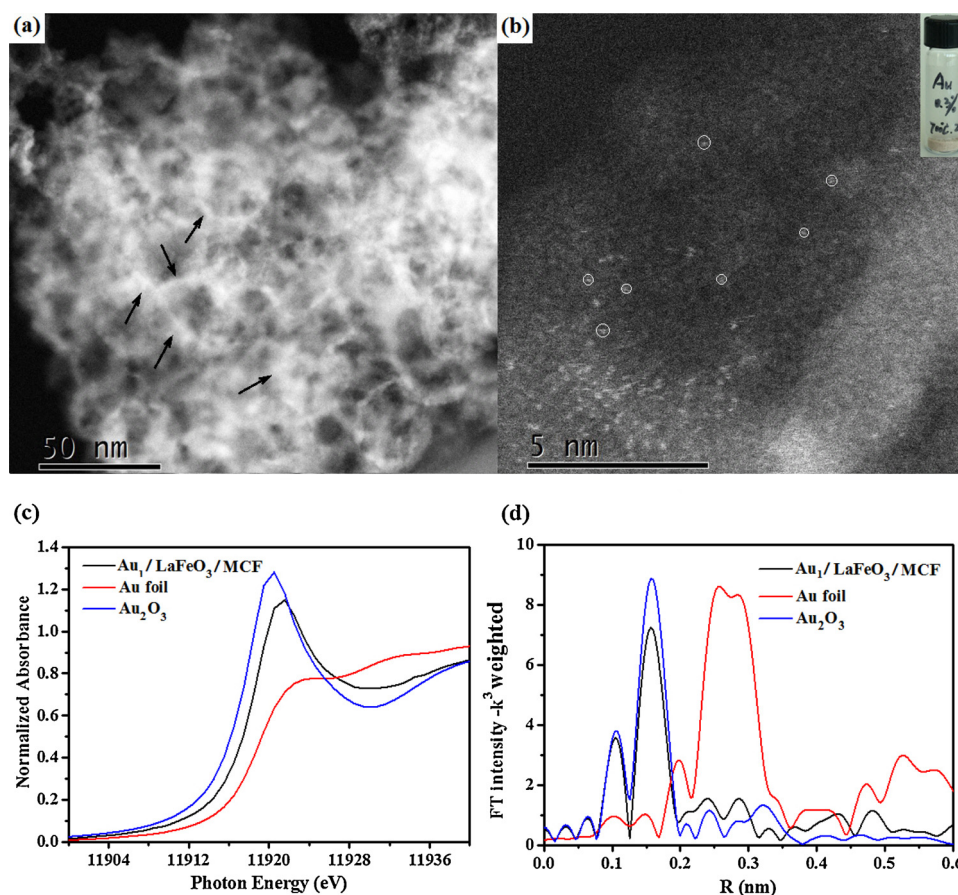
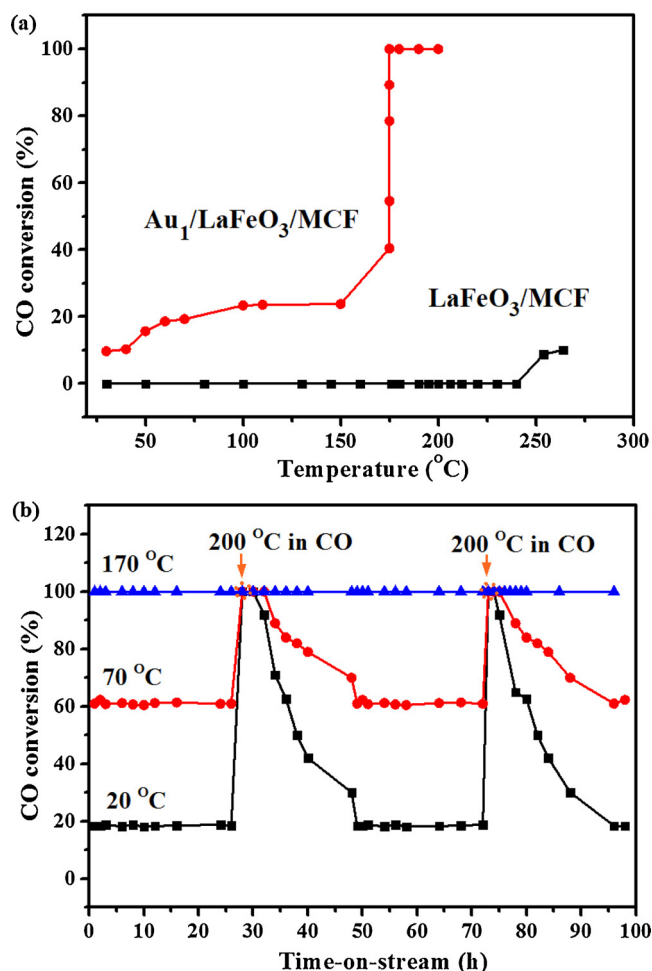


Fig. 2. (a) STEM image and (b) HAADF-STEM image of  $\text{Au}_1/\text{LaFeO}_3/\text{MCF}$ . (c) X-ray absorption near edge spectrum (XANES) of  $\text{Au}_1/\text{LaFeO}_3/\text{MCF}$ , Au foil and  $\text{Au}_2\text{O}_3$ . (d) Au LIII -edge EXAFS of  $\text{Au}_1/\text{LaFeO}_3/\text{MCF}$ , Au foil and  $\text{Au}_2\text{O}_3$ .



**Fig. 3.** (a) CO light-off curves of LaFeO<sub>3</sub>/MCF and the Au<sub>1</sub>/LaFeO<sub>3</sub>/MCF. (GHSV = 30,000 mL (h<sup>-1</sup> g<sub>cat</sub><sup>-1</sup>)). (b) Time-on-stream of CO oxidation rates over Au<sub>1</sub>/LaFeO<sub>3</sub>/MCF at 20 °C, 70 °C and 170 °C. (For interpretation of the references to colour in the text, the reader is referred to the web version of this article.)

third recycles also showed same “sudden change” and “plateau” before the sudden change. We hypothesized that the single Au atoms were highly saturated with oxygen species, and thereby blocking the adsorption the CO molecules, since the calcined Au<sub>1</sub>/LaFeO<sub>3</sub>/MCF was directly used for CO oxidation (red plot in Fig. 3a) without any further treatment. At higher reaction temperatures, the adsorbed oxygen species become unstable and desorb, giving rise to a significantly enhanced competitive adsorption of CO molecules.

In order to investigate the origins of the sudden increase in catalytic activity and verify the above proposed mechanism, the long-term *in operando* stability tests of the Au<sub>1</sub>/LaFeO<sub>3</sub>/MCF were studied at 20 °C, 70 °C, and 170 °C, with the results summarized in Fig. 3b. At room temperature, the 700 °C-calcined Au<sub>1</sub>/LaFeO<sub>3</sub>/MCF display a stable 18% CO conversion for the initial 24 h. By simply increasing the reaction temperature to 200 °C for 0.5 h on stream, the Au<sub>1</sub>/LaFeO<sub>3</sub>/MCF were activated and afforded a 100% conversion of CO. However, upon cooling to 20 °C, after affording a stable complete conversion of CO for the initial 3 h at 20 °C, the activity gradually decreased until plateauing at 18% conversion. When the reaction temperature was again increased to 200 °C and then allowed to cool to 20 °C, the Au SACs were again regenerated for several hours, with commensurate performance degradation observed, similar to the first catalyst activation. The activation mechanism is presumably similar to that proposed by Corma et al. [48] where small gold species (single atoms or clusters) promote dissociation of molecular O<sub>2</sub> and formation of a surface oxide layer. This

reaction is energetically favorable and occurs readily at room temperature, putatively resulting in the decline in activity for the Au<sub>1</sub>/LaFeO<sub>3</sub>/MCF. When the CO oxidation reaction was conducted at 70 °C (red plot in Fig. 3b), although a similar activation/deactivation profile was observed, less catalyst deactivation occurred as formation of adsorbed oxygen species on the single Au atoms is less favorable at 70 °C than at 20 °C. Nevertheless, as shown in Fig. 1 the deactivation pathway is fully reversible, enabling facile reactivation of Au<sub>1</sub>/LaFeO<sub>3</sub>/MCF by increasing the reaction temperature during the CO oxidation process. Furthermore, when the reaction temperature was as high as 170 °C, as shown in Fig. 3b (blue plot), the Au<sub>1</sub>/LaFeO<sub>3</sub>/MCF was very stable and showed no measurable decrease in performance over 90 h on stream.

The Au<sub>1</sub>/LaFeO<sub>3</sub>/MCF were characterized by XRD after CO oxidation and shown in Fig. S4. No diffraction peaks, associated with Au crystals, were observed, confirming that the atomically dispersed Au species did not aggregate to form Au clusters or NPs, even after the CO oxidation reaction. Aberration-corrected HAADF STEM images (Fig. 4) and the intensity profiles (Fig. S11) corroborated the absence of any Au clusters or NPs following CO oxidation catalysis, with only atomically dispersed Au atoms detected. The XAFS results of Au<sub>1</sub>/LaFeO<sub>3</sub>/MCF after CO oxidation supported existence of the oxygen-surrounded Au species and the lack of Au-Au interactions (Fig. S12). These complementary results firmly establish the sintering-resistance of perovskite-supported Au SACs.

In an effort to verify the oxidation state of the atomically dispersed Au species on the surfaces of the mesoporous perovskite support, *in situ* Fourier-transform infrared (FTIR) spectroscopy was employed to study the CO adsorption behavior (Fig. 5). Prior to testing the SACs, a control experiment was performed with the LaFeO<sub>3</sub>/MCF alone under the same reaction conditions with no appreciable CO adsorption observed on the support. In contrast, the Au<sub>1</sub>/LaFeO<sub>3</sub>/MCF displays a distinct band corresponding to adsorbed CO at 2215 cm<sup>-1</sup>. This sharp peak can be assigned to the adsorption of CO on a positively-charged Au species (Au<sup>3+</sup>) [49,50]. It implies that the surface Au active sites are predominately positively charged, consistent with the results observed by XANES.

### 3.3. Density functional theory (DFT) studies

DFT calculations were then carried out with the PBE functional to verify the oxidized Au species on the LaFeO<sub>3</sub> surface. We found stable adsorption of Au in the (001) O-hollow sites and in the Fe substituted vacancies, which match the observed Au–O bonding geometries. Overall, the adsorption of Au on the LaFeO<sub>3</sub> surfaces is stronger than on TiO<sub>2</sub>, supporting the observation of higher sintering resistance. The Au substituted site shown in Fig. 6 has an Au–O coordination of 4 with an average bond distance of ~2.2 Å, which is in perfect agreement with the results obtained by fitting the EXAFS data. This site is a very likely candidate for the active Au species on the real catalyst. A Bader charge analysis shows charge transfer from Au to O, yielding a positive charge of 0.78 |e| on Au. CO adsorption on the positively charged Au is strong, with an adsorption energy of -1.85 eV (Table S2) [51]. Therefore, the active centers for CO adsorption and oxidation are most likely to be the positive Au single-atom sites, in strong accordance with the FTIR and EXAFS results. We find O<sub>2</sub> cannot co-adsorb onto the CO-adsorbed Au single atom, which prevents CO oxidation via the Langmuir-Hinshelwood mechanism. Instead, facile CO oxidation can occur via the lattice oxygen of the LaFeO<sub>3</sub>, which we find has a vacancy formation energy of only 2.28 eV. The combination of strong CO adsorption and low vacancy formation are descriptors which can predict the facile conversion of CO to CO<sub>2</sub> via the Mars-van-Krevelen mechanism similar to other similar oxide systems [52,53].

## 4. Conclusions

In conclusion, the first successful synthesis of the new perovskite-

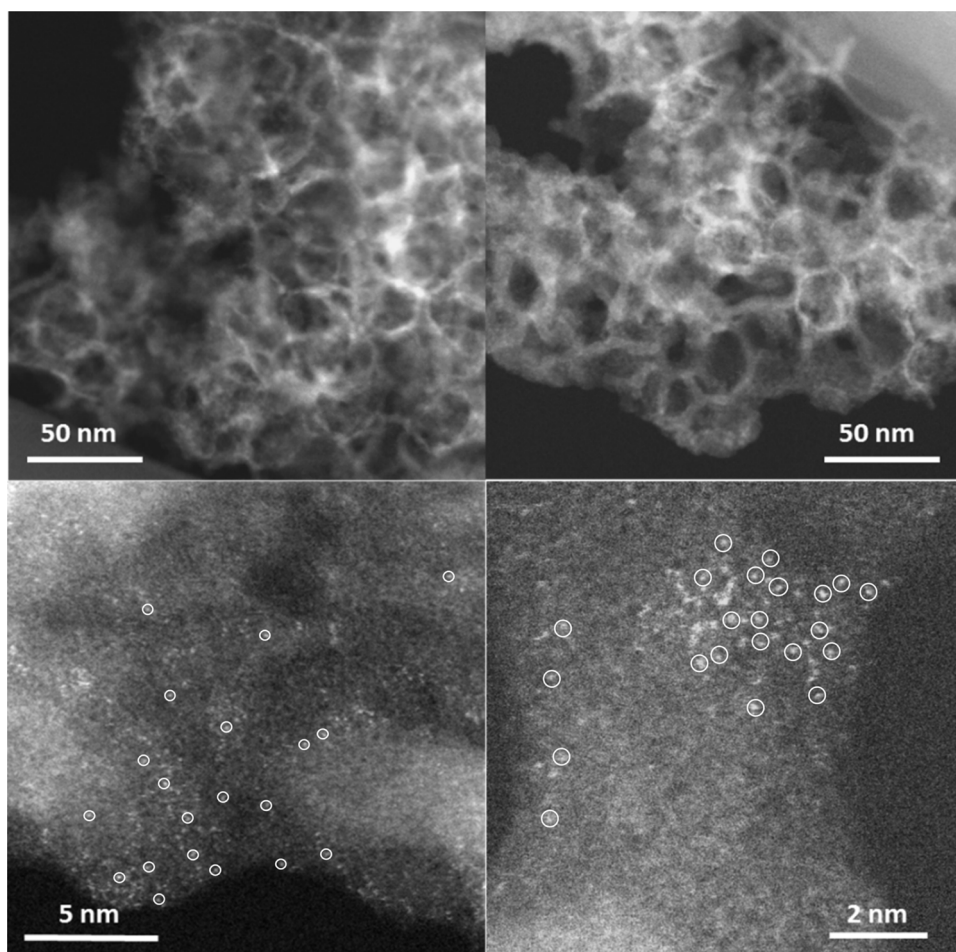


Fig. 4. Aberration-corrected HAADF-STEM images of the  $\text{Au}_1/\text{LaFeO}_3/\text{MCF}$  after CO oxidation ( $200^\circ\text{C}$ , 75 h, GHSV =  $30,000\text{ mL (h}^{-1}\text{ g}_{\text{cat}}^{-1})$ ).

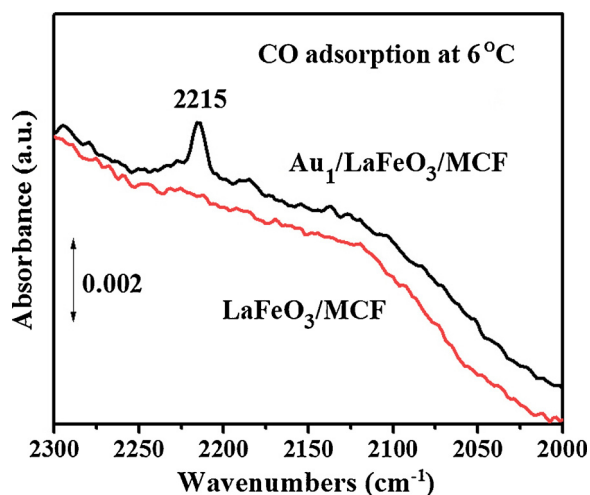


Fig. 5. FTIR spectra of CO adsorption at  $6^\circ\text{C}$  on the  $\text{LaFeO}_3/\text{MCF}$  and  $\text{Au}_1/\text{LaFeO}_3/\text{MCF}$ . The spectra were taken after purging the sample with He for 2 min.

stabilized Au SACs with remarkable thermal stability have been realized. Based on a high-surface-area heterostructured perovskite support,  $\text{Au}_1/\text{LaFeO}_3/\text{MCF}$  SACs were facilely prepared and demonstrated sintering-resistance after calcination in air at  $700^\circ\text{C}$  and under reaction conditions. Furthermore, the newly developed Au SACs possess high catalytic activity for CO oxidation and distinctively self-activation under reaction conditions. Both DFT calculations and experimental

analysis confirm that the surface Au active sites are predominately positively charged. For the current system, although we studied Au SACs as an example, we anticipate that this novel synthetic approach can be extended to other noble metals and work on expansion is currently underway in our lab.

#### Declaration of Competing Interest

The authors declare no competing financial interest.

#### Acknowledgments

The research was supported financially by US Department of Energy, Office of Science, Office of Basic Energy Sciences, Chemical Sciences, Geosciences, and Biosciences Division, Catalysis Science program. J.L. acknowledges support of the National Science Foundation under CHE-1465057 and the use of facilities in the John M. Cowley Center for High Resolution Electron Microscopy at Arizona State University. Use of the Stanford Synchrotron Radiation Lightsource, SLAC National Accelerator Laboratory, is supported by the US Department of Energy, Office of Science, Office of Basic Energy Sciences under Contract No. DE-AC02-76SF00515. Use of the National Energy Research Scientific Computing Center, a DOE Office of Science User Facility, is supported by the Office of Science of US Department of Energy under Contract No. DE-AC02-05CH11231. In situ FTIR studies and energy-dispersive X-ray spectroscopy (EDS) were conducted at the Center for Nanophase Materials Sciences, which is a DOE Office of Science User Facility. C.T. and H.Z. acknowledges support of Fundamental Research Funds for the Central Universities

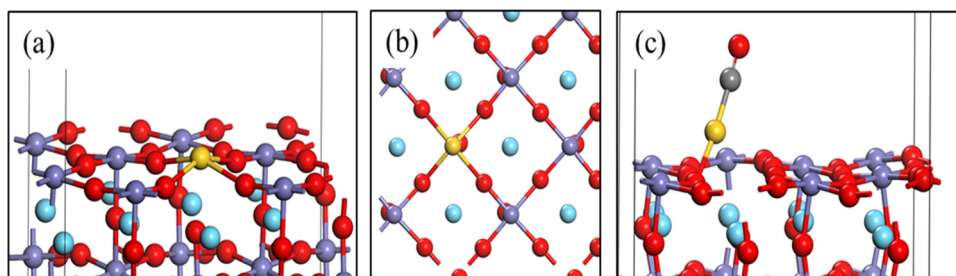


Fig. 6. DFT optimized structures for (a) side-view of Au/LaFeO<sub>3</sub> (100) (b) top-view of Au/LaFeO<sub>3</sub> (100) and (c) CO-adsorption geometry on Au/LaFeO<sub>3</sub> (100).

(50621021901007). X.Z. thanks the financial support from the Open Project of State Key Laboratory of Chemical Engineering (SKL-ChE-19C02) and the Young Thousand Talents Program.

## Appendix A. Supplementary data

Supplementary material related to this article can be found, in the online version, at doi:<https://doi.org/10.1016/j.apcatb.2019.118178>.

## References

- X. Cui, W. Li, P. Ryabchuk, K. Junge, M. Beller, Bridging homogeneous and heterogeneous catalysis by heterogeneous single-metal-site catalysts, *Nat. Catal.* 1 (2018) 385–397.
- L. Liu, A. Corma, Metal catalysts for heterogeneous catalysis: from single atoms to nanoclusters and nanoparticles, *Chem. Rev.* 118 (2018) 4981–5079.
- A. Wang, J. Li, T. Zhang, Heterogeneous single-atom catalysis, *Int. Rev. Chem. Eng.* 2 (2018) 65–81.
- M. Flytzani-Stephanopoulos, B.C. Gates, Atomically dispersed supported metal catalysts, *Annu. Rev. Chem. Biomol. Eng.* 3 (2012) 545–574.
- Y. Chen, S. Ji, C. Chen, Q. Peng, D. Wang, Y. Li, Single-atom catalysts: synthetic strategies and electrochemical applications, *Joule* 2 (2018) 1242–1264.
- X. Su, X.-F. Yang, Y. Huang, B. Liu, T. Zhang, Single-atom catalysis toward efficient CO<sub>2</sub> conversion to CO and formate products, *Acc. Chem. Res.* 52 (2019) 656–664.
- J. Jones, H. Xiong, A.T. DeLaRiva, E.J. Peterson, H. Pham, S.R. Challa, G. Qi, S. Oh, M.H. Wiebenga, X.I. Pereira Hernández, Y. Wang, A.K. Datye, Thermally stable single-atom platinum-on-ceria catalysts via atom trapping, *Science* 353 (2016) 150–154.
- B. Qiao, A. Wang, X. Yang, L.F. Allard, Z. Jiang, Y. Cui, J. Liu, J. Li, T. Zhang, Single-atom catalysis of CO oxidation using Pt<sub>1</sub>/FeOx, *Nat. Chem.* 3 (2011) 634–641.
- L. Nie, D. Mei, H. Xiong, B. Peng, Z. Ren, X.L.P. Hernandez, A. DeLaRiva, M. Wang, M.H. Engelhard, L. Kovarik, A.K. Datye, Y. Wang, Activation of surface lattice oxygen in single-atom Pt/CeO<sub>2</sub> for low-temperature CO oxidation, *Science* 358 (2017) 1419–1423.
- Z. Zhang, Y. Zhu, H. Asakura, B. Zhang, J. Zhang, M. Zhou, Y. Han, T. Tanaka, A. Wang, T. Zhang, N. Yan, Thermally stable single atom Pt/m-Al<sub>2</sub>O<sub>3</sub> for selective hydrogenation and CO oxidation, *Nat. Commun.* 8 (2017) 16100.
- X. Zhou, Q. Shen, K. Yuan, W. Yang, Q. Chen, Z. Geng, J. Zhang, X. Shao, W. Chen, G. Xu, X. Yang, K. Wu, Unraveling charge state of supported Au single-atoms during CO oxidation, *J. Am. Chem. Soc.* 140 (2018) 554–557.
- A.J. Therrien, A.J.R. Hensley, M.D. Marcinkowski, R. Zhang, F.R. Lucci, B. Coughlin, A.C. Schilling, J.-S. McEwen, E.C.H. Sykes, An atomic-scale view of single-site Pt catalysis for low-temperature CO oxidation, *Nat. Catal.* 1 (2018) 192–198.
- A. Corma, P. Concepción, M. Boronat, M.J. Sabater, J. Navas, M.J. Yacaman, E. Larios, A. Posadas, M.A. López-Quintela, D. Buceta, E. Mendoza, G. Guilera, A. Mayoral, Exceptional oxidation activity with size-controlled supported gold clusters of low atomicity, *Nat. Chem.* 5 (2013) 775–781.
- K. Ding, A. Gulec, A.M. Johnson, N.M. Schweitzer, G.D. Stucky, L.D. Marks, P.C. Stair, Identification of active sites in CO oxidation and water-gas shift over supported Pt catalysts, *Science* 350 (2015) 189–192.
- J. Zhang, L. Wang, B. Zhang, H. Zhao, U. Kolb, Y. Zhu, L. Liu, Y. Han, G. Wang, C. Wang, D.S. Su, B.C. Gates, F.-S. Xiao, Sinter-resistant metal nanoparticle catalysts achieved by immobilization within zeolite crystals via seed-directed growth, *Nat. Catal.* 1 (2018) 540–546.
- H. Wei, X. Liu, A. Wang, L. Zhang, B. Qiao, X. Yang, Y. Huang, S. Miao, J. Liu, T. Zhang, FeOx-supported platinum single-atom and pseudo-single-atom catalysts for chemoselective hydrogenation of functionalized nitroarenes, *Nat. Commun.* 5 (2014) 5634.
- J. Lin, A. Wang, B. Qiao, X. Liu, X. Yang, X. Wang, J. Liang, J. Li, J. Liu, T. Zhang, Remarkable performance of Ir<sub>1</sub>/FeOx single-atom catalyst in water gas shift reaction, *J. Am. Chem. Soc.* 135 (2013) 15314–15317.
- B. Qiao, J.-X. Liang, A. Wang, C.-Q. Xu, J. Li, T. Zhang, J.J. Liu, Ultrastable single-atom gold catalysts with strong covalent metal-support interaction (CMSI), *Nano Res.* 8 (2015) 2913–2924.
- J.-C. Liu, Y.-G. Wang, J. Li, Toward rational design of oxide-supported single-atom catalysts: atomic dispersion of gold on ceria, *J. Am. Chem. Soc.* 139 (2017) 6190–6199.
- Y. Kwon, T.Y. Kim, G. Kwon, J. Yi, H. Lee, Selective activation of methane on single-atom catalyst of rhodium dispersed on zirconia for direct conversion, *J. Am. Chem. Soc.* 139 (2017) 17694–17699.
- C.P. Canlas, J. Lu, N.A. Ray, N.A. Grosso-Giordano, S. Lee, J.W. Elam, R.E. Winans, R.P. Van Duyne, P.C. Stair, J.M. Notestein, Shape-selective sieving layers on an oxide catalyst surface, *Nat. Chem.* 4 (2012) 1030–1036.
- G.-H. Wang, J. Hilgert, F.H. Richter, F. Wang, H.-J. Bongard, B. Spliethoff, C. Weidenthaler, F. Schüth, Platinum–cobalt bimetallic nanoparticles in hollow carbon nanospheres for hydrogenolysis of 5-hydroxymethylfurfural, *Nat. Mater.* 13 (2014) 293–300.
- X.-Q. Gong, A. Selloni, O. Dulub, P. Jacobson, U. Diebold, Small Au and Pt clusters at the anatase TiO<sub>2</sub>(101) surface: behavior at terraces, steps, and surface oxygen vacancies, *J. Am. Chem. Soc.* 130 (2008) 370–381.
- D. Matthey, J.G. Wang, S. Wendt, J. Matthiesen, R. Schaub, E. Lægsgaard, B. Hammer, F. Besenbacher, Enhanced bonding of gold nanoparticles on oxidized TiO<sub>2</sub> (110), *Science* 315 (2007) 1692–1696.
- P. Liu, Y. Zhao, R. Qin, S. Mo, G. Chen, L. Gu, D.M. Chevrier, P. Zhang, Q. Guo, D. Zang, B. Wu, G. Fu, N. Zheng, Photochemical route for synthesizing atomically dispersed palladium catalysts, *Science* 352 (2016) 797–800.
- Y. Nishihata, J. Mizuki, T. Akao, H. Tanaka, M. Uenishi, M. Kimura, T. Okamoto, N. Hamada, Self-regeneration of a Pd-perovskite catalyst for automotive emissions control, *Nature* 418 (2002) 164–167.
- H. Tanaka, M. Taniguchi, M. Uenishi, N. Kajita, I. Tan, Y. Nishihata, J. Mizuki, K. Narita, M. Kimura, K. Kaneko, Self-regenerating Rh- and Pt-based perovskite catalysts for automotive-emissions control, *Angew. Chem. Int. Ed.* 45 (2006) 5998–6002.
- T.M. Onn, M. Monai, S. Dai, E. Fonda, T. Montini, X. Pan, G.W. Graham, P. Fornasiero, R.J. Gorte, Smart Pd catalyst with improved thermal stability supported on high-surface-area LaFeO<sub>3</sub> prepared by atomic layer deposition, *J. Am. Chem. Soc.* 140 (2018) 4841–4848.
- C. Tian, X. Zhu, C.W. Abney, X. Liu, G.S. Foo, Z. Wu, M. Li, H.M. Meyer, S. Brown, S.M. Mahurin, S. Wu, S.-Z. Yang, J. Liu, S. Dai, Toward the design of a hierarchical perovskite support: ultra-sintering-resistant gold nanocatalysts for CO oxidation, *ACS Catal.* 7 (2017) 3388–3393.
- J.L. Rogers, M.C. Mangarella, A.D. D'Amico, J.R. Gallagher, M.R. Dutzler, E. Stavitski, J.T. Miller, C. Sievers, Differences in the nature of active sites for methane dry reforming and methane steam reforming over nickel aluminate catalysts, *ACS Catal.* 6 (2016) 5873–5886.
- C. Tian, S.-H. Chai, X. Zhu, Z. Wu, A. Binder, J.C. Bauer, S. Brwon, M. Chi, G.M. Veith, Y. Guo, S. Dai, In situ growth synthesis of heterostructured LnPO<sub>4</sub>-SiO<sub>2</sub> (Ln = La, Ce, and Eu) mesoporous materials as supports for small gold particles used in catalytic CO oxidation, *J. Mater. Chem.* 22 (2012) 25227–25235.
- M.S. Nashner, A.I. Frenkel, D.L. Adler, J.R. Shapley, R.G. Nuzzo, Structural characterization of carbon-supported platinum–ruthenium nanoparticles from the molecular cluster precursor PtRu<sub>5</sub>C(CO)<sub>16</sub>, *J. Am. Chem. Soc.* 119 (1997) 7760–7771.
- B. Ravel, M. Newville, ATHENA, ARTEMIS, HEPHAESTUS: data analysis for X-ray absorption spectroscopy using IFEFFIT, *J. Synchrotron Radiat.* 12 (2005) 537–541.
- G. Kresse, J. Furthmüller, Efficiency of ab-initio total energy calculations for metals and semiconductors using a plane-wave basis set, *Comput. Mater. Sci.* 6 (1996) 15–50.
- G. Kresse, J. Furthmüller, Efficient iterative schemes for ab initio total-energy calculations using a plane-wave basis set, *Phys. Rev. B* 54 (1996) 11169–11186.
- J.P. Perdew, K. Burke, M. Ernzerhof, Generalized gradient approximation made simple, *Phys. Rev. Lett.* 77 (1996) 3865–3868.
- P.E. Blöchl, Projector augmented-wave method, *Phys. Rev. B* 50 (1994) 17953–17979.
- H.J. Monkhorst, J.D. Pack, Special points for Brillouin-zone integrations, *Phys. Rev. B* 13 (1976) 5188–5192.
- D. Friebe, D.J. Miller, C.P. O'Grady, T. Anniyev, J. Bargar, U. Bergmann, H. Ogasawara, K.T. Wikfeldt, L.G.M. Pettersson, A. Nilsson, In situ X-ray probing reveals fingerprints of surface platinum oxide, *Phys. Chem. Chem. Phys.* 13 (2011) 262–266.
- T.A. Petach, M. Lee, R.C. Davis, A. Mehta, D. Goldhaber-Gordon, Mechanism for the large conductance modulation in electrolyte-gated thin gold films, *Phys. Rev. B* 90 (2014) 081108.
- J.J. Rehr, R.C. Albers, Theoretical approaches to x-ray absorption fine structure,

- Rev. Mod. Phys. 72 (2000) 621–654.
- [42] D. Gu, J.-C. Tseng, C. Weidenthaler, H.-J. Bongard, B. Spliethoff, W. Schmidt, F. Soulimani, B.M. Weckhuysen, F. Schüth, Gold on different manganese oxides: ultra-low-temperature CO oxidation over colloidal gold supported on Bulk-MnO<sub>2</sub> nanomaterials, *J. Am. Chem. Soc.* 138 (2016) 9572–9580.
- [43] C. Hardacre, T. Rayment, R.M. Lambert, Platinum/Ceria CO oxidation catalysts derived from Pt/Ce crystalline alloy precursors, *J. Catal.* 158 (1996) 102–108.
- [44] L.-W. Guo, P.-P. Du, X.-P. Fu, C. Ma, J. Zeng, R. Si, Y.-Y. Huang, C.-J. Jia, Y.-W. Zhang, C.-H. Yan, Contributions of distinct gold species to catalytic reactivity for carbon monoxide oxidation, *Nat. Commun.* 7 (2016) 13481.
- [45] X. Xu, Q. Fu, X. Guo, X. Bao, A highly active “NiO-on-Au” surface architecture for CO oxidation, *ACS Catal.* 3 (2013) 1810–1818.
- [46] J. Guzman, B.C. Gates, Catalysis by supported gold: correlation between catalytic activity for CO oxidation and oxidation states of gold, *J. Am. Chem. Soc.* 126 (2004) 2672–2673.
- [47] X.-N. Li, Z. Yuan, S.-G. He, CO oxidation promoted by gold atoms supported on titanium oxide cluster anions, *J. Am. Chem. Soc.* 136 (2014) 3617–3623.
- [48] L. Alves, B. Ballesteros, M. Boronat, J.R. Cabrero-Antonino, P. Concepción, A. Corma, M.A. Correa-Duarte, E. Mendoza, Synthesis and stabilization of subnanometric gold oxide nanoparticles on multiwalled carbon nanotubes and their catalytic activity, *J. Am. Chem. Soc.* 133 (2011) 10251–10261.
- [49] Z. Wu, D.-e. Jiang, A.K.P. Mann, D.R. Mullins, Z.-A. Qiao, L.F. Allard, C. Zeng, R. Jin, S.H. Overbury, Thiolate ligands as a double-edged sword for CO oxidation on CeO<sub>2</sub> supported Au<sub>25</sub>(SCH<sub>2</sub>CH<sub>2</sub>Ph)<sub>18</sub> nanoclusters, *J. Am. Chem. Soc.* 136 (2014) 6111–6122.
- [50] Z. Wu, S. Zhou, H. Zhu, S. Dai, S.H. Overbury, DRIFTS-QMS study of room temperature CO oxidation on Au/SiO<sub>2</sub> catalyst: nature and role of different Au species, *J. Phys. Chem. C* 113 (2009) 3726–3734.
- [51] M.F. Camellone, S. Fabris, Reaction mechanisms for the CO oxidation on Au/CeO<sub>2</sub> catalysts: activity of substitutional Au<sup>3+</sup>/Au<sup>+</sup> cations and deactivation of supported Au<sup>+</sup> adatoms, *J. Am. Chem. Soc.* 131 (2009) 10473–10483.
- [52] C. Wang, X.-K. Gu, H. Yan, Y. Lin, J. Li, D. Liu, W.-X. Li, J. Lu, Water-mediated Mars–Van Krevelen mechanism for CO oxidation on ceria-supported single-atom Pt<sub>1</sub> catalyst, *ACS Catal.* 7 (2017) 887–891.
- [53] H.Y. Kim, G. Henkelman, CO oxidation at the interface of Au nanoclusters and the stepped-CeO<sub>2</sub>(111) surface by the Mars–van Krevelen mechanism, *J. Phys. Chem. Lett.* 4 (2013) 216–221.